Commissioning ‘Opihi: a wide-angle finderscope for the NASA Infrared Telescope Facility

Ellen Lee[a], Kenji S. Emerson[a], Michael S. Connelley[a], Theodora Bowe[b], Schelte J. Bus[a], and Charles Z. Lockhart[a]

[a]Institute for Astronomy, 640 N. Aohoku Place, Hilo, HI 96720, USA
[b]Institute for Astronomy, 2680 Woodlawn Drive, Honolulu, HI 96822, USA

ABSTRACT

‘Opihi is a 0.43 m, 32′ field of view (FOV) finderscope that rides along with the NASA Infrared Telescope Facility (IRTF), a 3.2 m infrared-optimized telescope near the summit of Mauna Kea, Hawai‘i. The main purpose of ‘Opihi is to recover Near-Earth Objects (NEOs) with positional uncertainties larger than can feasibly be found with the 1′ FOV of IRTF. Automated data collection with ‘Opihi will be useful for bootstrap photometry and can provide general context observing images. We present the design and commissioning process for ‘Opihi, including its photometric performance and first asteroid detection results.

Keywords: Wide-Field Imaging, Planetary Defense, Infrared Astronomy, Ground-Based Astronomy.

1. INTRODUCTION

Asteroids are the remnants of planetary formation in the Solar System. Reflectance spectroscopy of asteroids allows them to be grouped into different taxonomic classes based on their spectral features.[1,2] Asteroids with similar orbits can also be placed into families, which may have originated from collisions between larger parent bodies.[3] By combining spectroscopic and orbital information obtained from asteroids, we can understand the conditions of the early Solar System and how they may have impacted the formation of the planets.[4] NEOs make natural targets for space missions because they are easy to reach and are also a major source of meteorites. It is also important to characterize NEOs from the ground in the context of impact risk assessment.[5]

Planetary defense is a priority of the IRTF. The prism mode (0.70-2.52 µm, $R \sim 200$) of the IRTF’s low- to medium-resolution infrared spectrograph SpeX[6] is most often used to take asteroid spectra. As an object approaches the Earth, its positional uncertainty on the sky increases drastically. If this uncertainty is too large, it becomes difficult to locate the object in the 1′ field of view (FOV) of SpeX, making it impossible to perform follow-up spectroscopic observations.

We have created ‘Opihi for the main purpose of recovering such NEOs that currently cannot be recovered by the IRTF. The main body of ‘Opihi is a commercially manufactured telescope that is mounted to the side of the IRTF. ‘Opihi’s name is derived from the Hawaiian name for *Cellana exarata*, a limpet that firmly attaches itself to seaside rocks. It is capable of functioning independently and can be used in parallel with facility instruments. In this paper, we present the design of ‘Opihi and its accompanying software, which can be used to propagate the location of an asteroid into the future. The software can also perform active and/or passive reduction of ‘Opihi images. We also discuss the commissioning process for ‘Opihi, including alignment to the IRTF, photometric performance, and asteroid detection.

Further author information: (Send correspondence to E.L.)
E.L.: E-mail: ellenlee@hawaii.edu
K.S.E.: E-mail: kemerson@hawaii.edu

Table 1: A summary of instrument characteristics.

‘Opihi	
Diameter	0.43 m
Field of View	$32'$
Pixel Scale	$0.94''$/pixel
Filters	g’, r’, i’, z’, clear
Detector (CCD)	
Bandpass	360 - 970 nm
Format (Pixels)	2048×2048
Operating Temperature	$-50\,^{\circ}$C
Dark Current	1 e^-/s
Read Noise (5 MHz)	41.2 e^- rms
Well Depth	128,245 e^-

2. INSTRUMENT OVERVIEW

Figure 1 shows the assembled ‘Opihi mounted to the IRTF, with Fig 2 for scale. ‘Opihi consists of a 0.43 m corrected Dall-Kirkham telescope manufactured by PlaneWave Instruments*. Together with its 2k × 2k CCD camera, it achieves a FOV of $32'$ and enough sensitivity to recover a 20th magnitude object in one minute. ‘Opihi uses four SDSS filters[7] (g’, r’, i’, z’) and a clear position. This permits ‘Opihi images to be used for absolute spectral flux calibration because the i’ and z’ filters overlap with the 0.70-2.52 µm spectral modes of SpeX. Table 1 contains more information about relevant system parameters.

A rectangular shell encloses ‘Opihi along with its electronics to provide shielding from the environment. Additionally, ‘Opihi is equipped with a cover for protection while not in use. More importantly, since IRTF may be used for daytime observing, it is necessary to protect ‘Opihi from focusing the Sun’s light and becoming a fire hazard.

The IRTF must be tilted south to a declination of -50° in order to access the mounting point. For installation, we use a cradle that holds ‘Opihi at a fixed 20° angle. A tip/tilt stage is attached to ‘Opihi to allow for alignment with the IRTF. Then, an interface plate is attached to the tip/tilt stage so that ‘Opihi can be mounted to the IRTF. Alignment is necessary because the optical axes of ‘Opihi and the IRTF do not overlap with each other after installation.

3. DATA REDUCTION

3.1 Software Framework

To accomplish the desired objectives of the ‘Opihi telescope, for each image, we need to determine the astrometric plate solution, the photometric calibration, a preliminary orbit, an ephemeris calculation, and the on-sky asteroid motion propagation. Different packages and services have solved these problems. The overarching objective of the software data reduction package is to interface with these separate services and leverage them to process ‘Opihi data and present both the controls and the results to a user via a unified graphical user interface (GUI). (The software repository for OpihiExarata can be found on Github†.)

Because each service has its own unique application programming interface (API), each of our backend interfaces also are different. We abstract their APIs, creating a wrapper that allows us to interact with their inputs and outputs without having to manage the intricacies of each service, so that we can better interface with

*https://planewave.com/

†https://github.com/psmd-iberutaru/OpihiExarata

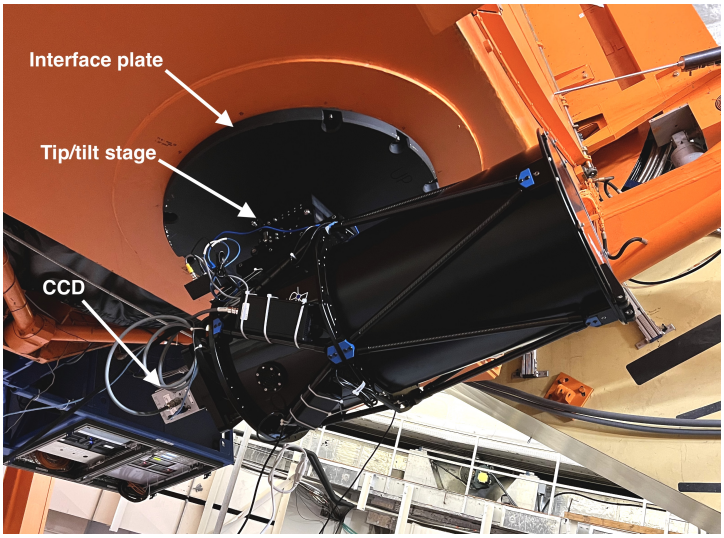

Figure 1: ‘Opihi mounted to the side of IRTF before the installation of the protective shell. The telescope cover’s piston is not present because it was removed for repairs. To access the mounting point and ‘Opihi, the IRTF is pointed south (Dec = −50°) as shown in this image.

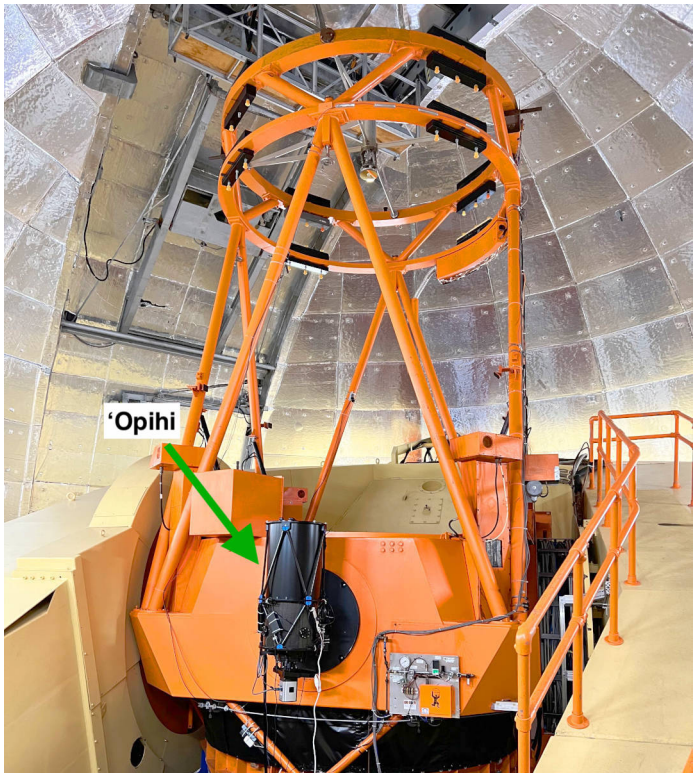

Figure 2: A full view of ‘Opihi together with the IRTF pointing near zenith.

them with our software. There are multiple ways the smaller problems could be solved (e.g. different photometric databases) and so each has its own abstraction layer. Currently, our primary implementations are as follows:

For astrometric plate solving, we utilize Astrometry.net,[8] either the online version[‡] or a local installation. It compares the position of stars in an image with the known location of stars from an astrometric database (like the Gaia DR 2 database[9]) to determine the astrometric solution.

For photometric solving, we utilize the Pan-STARRS 3π PS1 survey (data release 2)[10] photometric database. We selected this database because it has a similar sky coverage to the IRTF and also uses filters similar to the ʻOpihi filters. We query their database for the positions and filter magnitudes of stars within the ʻOpihi field of view using the MAST toolkit[§].

For preliminary orbit solving, we utilize the OrbFit software package.[11] We determined this to be the best documented preliminary orbit calculator available at the time that fit well for our purposes. It calculates the orbital elements of asteroids when provided with observations in the MPC 80-column format. A user may supersede OrbFit by providing their own custom Keplerian orbital elements.

For ephemerides calculations, we utilize the JPL Horizons service.[12] The IRTF already has many tools relying on the JPL Horizons service so it is natural that OpihiExarata uses it as well. When provided with the Keplarian orbital elements, it returns an ephemeris for a future time.

For asteroid position propagation, we utilize an in-house implementation of a linear extrapolation of the asteroid's position. We use multiple images over a short time to determine the on-sky motion of the asteroid and linearly propagate forward in time, ignoring higher order effects.

We decided to allow for similar services (e.g. similar astrometric plate solver services) to be interchangeable with each other; in the event that one is inadequate, the user may pick another from the GUI. The above listed services are just the default services we use to determine the astrometric, photometric, orbital, ephemeris, and propagation solutions. Additional services will be made available in the future (see Sec. 5).

3.2 Usage Procedure

The two main functions of the ʻOpihi telescope are to serve as an asteroid viewfinder and a photometric monitor.

In its asteroid viewfinder mode, the user (typically a telescope operator or an astronomer) specifies the name of the (to be observed) asteroid and takes an image. Once loaded, the user finds the asteroid in the image by comparing it to a previous image. After an astrometric solution is derived, the asteroid's on-sky position is known. A photometric solution may also be determined. Using historical observations (either previous images or archival observations from the Minor Planet Center), we can solve for the orbital elements and an ephemeris to determine its future position. Alternatively, using previous images, a quick propagation solution can also determine the future position of an asteroid. In either case, an asteroid's future on-sky track can be sent to the telescope control system to correctly point to the asteroid. A flow chart of the asteroid viewfinding process is shown in Fig. 3a.

In its photometric monitoring mode, the user (typically a telescope operator) triggers the ʻOpihi camera controller to take images repeatedly at regular intervals. They also specify the directory that these repeated images are being saved to before triggering OpihiExarata to automatically solve them. The software automatically fetches the most recently taken image and processes it using the calibration images we took (see the end of Sec. 4.1). It then solves for the astrometric solution then photometric solution of the processed image. The processed image, along with its astrometric and photometric results, are saved to the disk. From the photometric solution, the magnitude zero point of the image is also recorded to a database containing current and past measurements. Using this zero point data, the software updates a web page that serves as a sky transparency monitor. The process of taking an image then fetching, processing, and solving it to update a zero point database and monitoring web page is repeated automatically until stopped by the user. A flowchart of the photometric monitoring process is diagrammed in Fig. 3b.

[‡]The online version can be found at `https://nova.astrometry.net/`.

[§]More generally, the Pan-STARRS querying infrastructure comes from the Mikulski Archive for Space Telescopes (MAST) service, `https://catalogs.mast.stsci.edu/panstarrs/`.

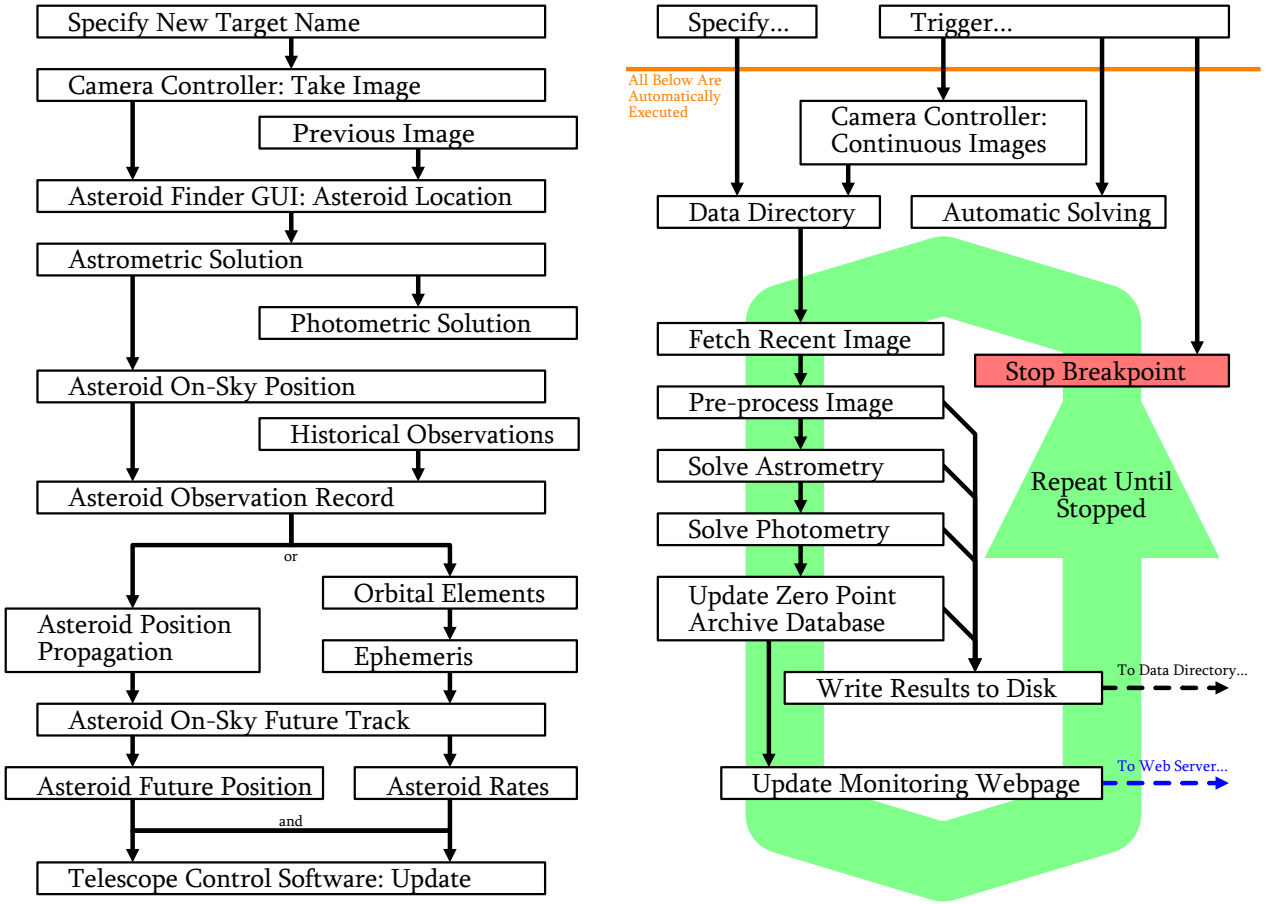

(a) For the asteroid viewfinder mode.

(b) For the photometric monitoring mode.

Figure 3: These are visual diagrams of the workflow procedures of the OpihiExarata software as detailed in 3.2. The two different workflows correspond to the two main functions of the ‘Opihi telescope.

4. ON-SKY TESTING

4.1 Installation

Refer to Tab. 2 for a timeline of the commissioning process. ‘Opihi was installed on the IRTF in mid-February.

The first night of engineering was used to confirm basic functionality. ‘Opihi is controlled in a similar manner to other IRTF instruments, which includes a GUI to command the camera and filter wheel along with a data viewer to display images. An arbitrary star field in the south was used to verify collimation and focus the telescope. That night, seeing on Mauna Kea was 0.9″, so ‘Opihi was focused until the (unsaturated) stars became point-like. The seeing is normally smaller than the pixel scale when the weather is good. Using an astrometric solution of the star field, we then determined that the offset between the center of ‘Opihi’s and IRTF’s FOVs was 10′ north and 45′ west. We also measured the pixel scale to be 0.94″/pixel and the camera rotation to be 7°.

Table 2: The commissioning timeline during the Spring of 2022. Each date represents the start date of a block of observing time. We have used 10 engineering nights in total.

02/19	First light. Basic functionality and camera offset through astrometry.
03/12	Alignment to IRTF. Photometric data with z’. Coarse flexure measurements.
03/31	Photometric data across all filters. Detector linearity tests to saturation.
04/07	Adjusting camera settings. First asteroid data.
04/24	Asteroid location tests. Using ‘Opihi together with SpeX.

IRTF was kept south for most of our first light observations because we found that the dome slit clipped ‘Opihi’s beam. To get around this, we added an option to offset IRTF’s dome slit while observing with ‘Opihi; the slit is typically centered on IRTF’s beam, but the offset makes it so that it is instead centered on the midpoint between IRTF and ‘Opihi. There was no vignetting of IRTF or ‘Opihi after correctly applying the offset.

Next, we aligned ‘Opihi so that the 1′ FOV of SpeX’s guiding cameras would appear near the center of ‘Opihi’s 32′ FOV. To access the tip/tilt stage, we guided the IRTF on a pre-selected star that was transiting in the south (around a declination of −50° as before). Two individuals climbed onto the platform to adjust the tip/tilt stage while another person used the astrometric solution to determine the location of the star relative to the FOV of ‘Opihi. Adjustments made through the tip/tilt stage were correlated to physical movements on the sky with trigonometry. Within about an hour, we were able to get the star within a 5″ of the center of ‘Opihi’s FOV.

The alignment allowed us to point ‘Opihi to specific targets more consistently. Due to ‘Opihi’s large FOV, a few arcminutes of flexure in any direction is permissible. The IRTF was pointed at nine different locations on the sky which were equally spaced between declinations of −25° to 60° and hour angles of -3^{h} to 3^{h}. There is no one-to-one correspondence between changes in the flexure and changes in the position of IRTF, which is most likely due to hysteresis in the mercury retaining ring holding its primary mirror.[13] We found that ‘Opihi’s FOV drifted by a maximum of around 1′.

Although we began to take photometric data at this point, several other tests were done on the camera by taking calibration frames. Photometric performance is detailed in Sec. 4.2. We first attempted to take sky flats at twilight; to avoid saturation, the exposure time was just a few seconds. This degraded the quality of these flats because the pattern of the CCD’s moving shutter appeared in the final image. Ultimately, we found that the best way to take flats was to place an illuminated translucent screen in front of ‘Opihi. The flats taken with this method were of good quality and were thus used for data reduction.

By taking the median counts of flats with increasing exposure times, we measured that the linearity of the detector was within 0.2 % of the full well depth. The dark current was similarly well-behaved. A bad pixel map was also created using the flats and darks. Pixels with counts that were 5σ above the median dark counts were deemed hot pixels. Likewise, pixels with counts below 5σ of the median in the flats were counted as dead pixels.

Table 3: Filter wheel positions. The zero point and limiting magnitude $m_{\rm lim}$ are computed from the data. They correspond to a quarter moon with clear weather along with $S/N = 60$ at an exposure time of $t = 60\,\mathrm{s}$. Poor observing conditions can degrade $m_{\rm lim}$ by around half a magnitude or greater.

Filter	Zero point	$m_{\rm lim}$
g'	21.6	18.5
r'	21.2	18.3
i'	21.1	18.0
z'	20.5	17.2
clear	22.5	20.1

With these criteria, we determined that there were 1023 pixels with unacceptably high dark current and just one dead pixel. We also found that the camera was able to hold the temperature of $-50\,^{\circ}\mathrm{C}$ steady within $1\,^{\circ}\mathrm{C}$.

4.2 Photometric performance

The Sloan Digital Sky Survey[14] and Pan-STARRS[15] cover most regions of the sky observable from Mauna Kea and use the same filters as ‘Opihi. Thus, we targeted star fields that were covered by at least one of these surveys. Even if observing conditions were not ideal, the large number of stars in a given ‘Opihi image provided many references with which we could do photometry.

The results of our test photometry are provided in Tab. 3. A standalone Python script was written to reduce test photometric data on individual stars. As outlined in Sec. 3.1, OpihiExarata will be used to perform photometry on ‘Opihi data for general use. Given photometric weather, the zero point for each filter was typically stable within 0.07 magnitudes across one exposure. ‘Opihi is least efficient in the z'-band because the decreasing quantum efficiency of the detector at longer wavelengths. The sensitivity is highest for the g' filter, but is comparable across r' and i' as well.

Limiting magnitudes were also estimated by computing the signal-to-noise of multiple stars across different nights. Because the magnitude is known for each star, it is possible to estimate the flux density required to yield any desired signal-to-noise. $S/N = 60$ was chosen as a rough limit of what can be detected by eye in a processed image. Due to under-sampling, most of the signal is concentrated on the central pixel of the target; it becomes difficult to locate a target if the visible signal is confined to a single pixel, even if the signal-to-noise appears to be serviceable. The clear position will be used for detecting asteroids because it is the most sensitive under our expected observing conditions. There is no real way to define a magnitude without using filters, but a “clear magnitude” was estimated by averaging the fluxes of the four filters.

We were also able to create four-color images using the photometric data. Figure 4 shows a colored image of the galaxies M65 and M66 taken by ‘Opihi and processed with GIMP. Exposures taken through each of the four filters provided the colors while the brightness of each pixel was determined by a composite image of several clear exposures summed together. Before colorizing the image in GIMP, each frame was processed through flat fielding and subtracting out the dark current along with the median sky background. The color map roughly correlates g' to blue, r' to green, i' to yellow, and z' to red with some changes to the brightness and saturation of each color.

4.3 Asteroid observations with ‘Opihi

The general process for observing asteroids with ‘Opihi begins with pointing the IRTF to the expected location of the object. The asteroid must then be located in several images of the star field so that our astrometric solution (refer to Sec. 3) can be used to propagate the coordinates into the future. After the IRTF is pointed to this location on the sky, the asteroid can be located in the $1'$ FOV of SpeX's guiding cameras so that a spectrum can be taken.

Figure 4: A colorized image of the galaxy pair M65 and M66 created from ‘Opihi data. The illumination frame–which determined the brightness of each pixel–consisted of ten $t = 30\,\mathrm{s}$ clear images to mitigate CCD blooming for the brightest stars. This frame was colorized with one $t = 60\,\mathrm{s}$ exposure from each filter.

Asteroids differentiate themselves from the background stars in an image via their non-sidereal motion. Provided that there is a good signal, it is relatively straightforward to visually locate an asteroid in an A-B subtracted image pair. There are two ways to generate such a pair. First, one can guide on a background star and subtract two exposures. Alternatively, one can guide at non-sidereal rates, which would require an offset to one of the images before subtraction.

Figure 5 shows A-B pairs obtained using both methods. It is often preferable to guide at non-sidereal rates when searching for fainter, faster objects—constituting most of ‘Opihi’s targets—because it prevents the signal from being smeared across several pixels. However, it is occasionally useful to guide at sidereal rates because subtracting A-B images without an offset is slightly easier, and can be done automatically in ‘Opihi’s data viewer.

We began testing the asteroid finding capabilities of ‘Opihi before the frontend of OpihiExarata was finished, but our workflow was similar to what can be exercised by one observer in the future. For initial testing, we observed bright, well-known asteroids. After confirming that all necessary components were functioning—finding the asteroid in ‘Opihi’s FOV, ephemeris propagation, and placing the asteroid in SpeX’s slit—we targeted fainter, newer objects. Ephemerides for our targets were drawn from the JPL Small-Body Database. We also selected targets from the Minor Planet Center’s Near-Earth Object Confirmation Page,[16] which updates continuously with the most recent (i.e., same day) potential NEO detections.

As shown in Fig. 5b, we were able to locate the 20th magnitude asteroid 2022 HP1. We were also able to propagate the ephemeris with enough precision that it could be located within the FOV of SpeX. We found that locating the asteroid in each image, solving astrometry, and computing the propagated coordinates could be done around 15 minutes.

For example, Fig. 6 shows the difference between the propagated trajectory of the asteroid 2022 HB and its JPL ephemeris as a function of time. A deviation of a few arcseconds is acceptable given that the FOV of SpeX is $1'$. Our biggest limitation came from the overhead time between propagation and slewing the telescope to the target. The ephemeris propagation works by extrapolating the position of the asteroid in several exposures into

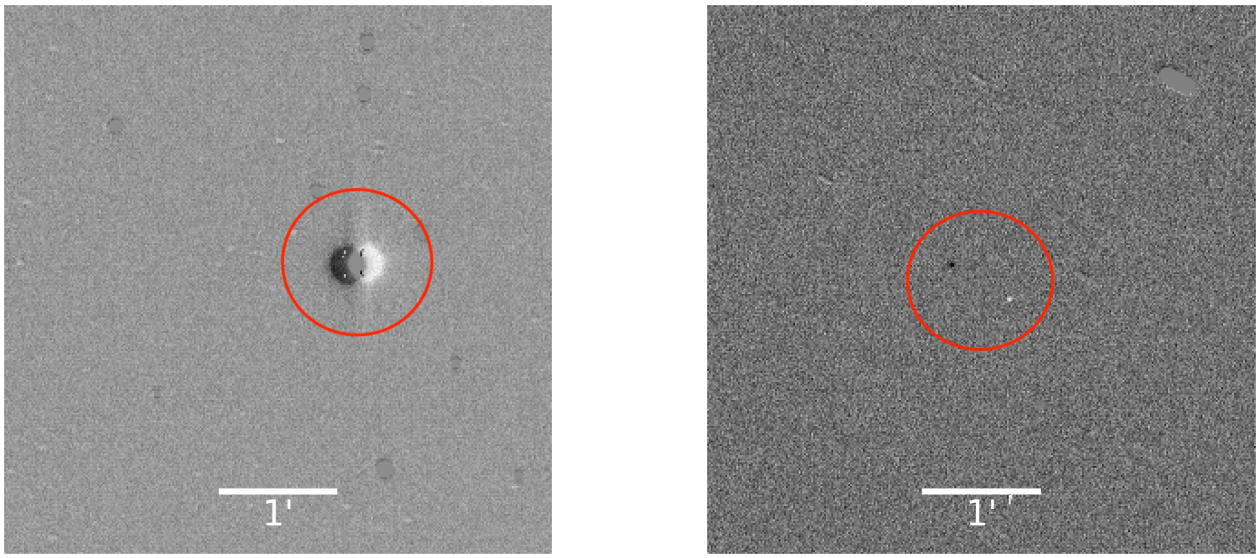

(a) Sidereal guiding

(b) Non-sidereal guiding

Figure 5: A-B subtracted pairs for two asteroids, each circled in red. The images are cropped for clarity. (a) Asteroid 7 Iris ($V \sim 10.5$) at an exposure time of $t = 20\,\mathrm{s}$. The two frames used for this subtraction were taken around half an hour apart from each other. The asteroid is easily identified by the fact that it is moving with a different rate from the background stars. The background stars, which have been subtracted off, appear as residual circles. (b) 2022 HP1 ($V \sim 20$) at $t = 90\,\mathrm{s}$, where $S/N = 90$ for this detection. This object had a much higher non-sidereal rate of $0.1''/\mathrm{s}$; the exposures used for this pair were taken three minutes apart. Residual streaks from the subtracted background stars are present.

some specified time in the future. If the selected time was off from the actual observation time of the asteroid by a few minutes, the asteroid would drift far enough from the predicted location that it could not be recovered in the FOV of SpeX. Improvements to the frontend of the software and using a locally hosted version of Astrometry.net will significantly reduce the overhead time. Eventually, the software will directly pass the projected ephemeris to the telescope control system, further minimizing overhead.

5. CONCLUSIONS AND FUTURE WORK

We have demonstrated that ‘Opihi can be used for its primary objective of recovering recently discovered NEOs. Asteroid observations from ‘Opihi will added to the Minor Planet Center database, reducing their positional uncertainties and thus improving our knowledge of their orbital parameters and ephemerides. We plan to implement passive observing modes, including a sky extinction monitor similar to the Canada-France-Hawaii Telescope’s SkyProbe.[17] Since it can be used in parallel with facility instruments, photometric data can be taken continuously by ‘Opihi for absolute flux calibration of SpeX data; it can also unobtrusively take general context images for observers when other observing modes are not needed.

ACKNOWLEDGMENTS

We would like to thank John T. Rayner for helpful feedback and discussions regarding ‘Opihi.

The Infrared Telescope Facility is operated by the University of Hawaii under contract 80HQTR19D0030 with the National Aeronautics and Space Administration. This project has made use of the Minor Planet & Comet Ephemeris Service (IAU Minor Planet Center) This work has made use of data from the European Space Agency

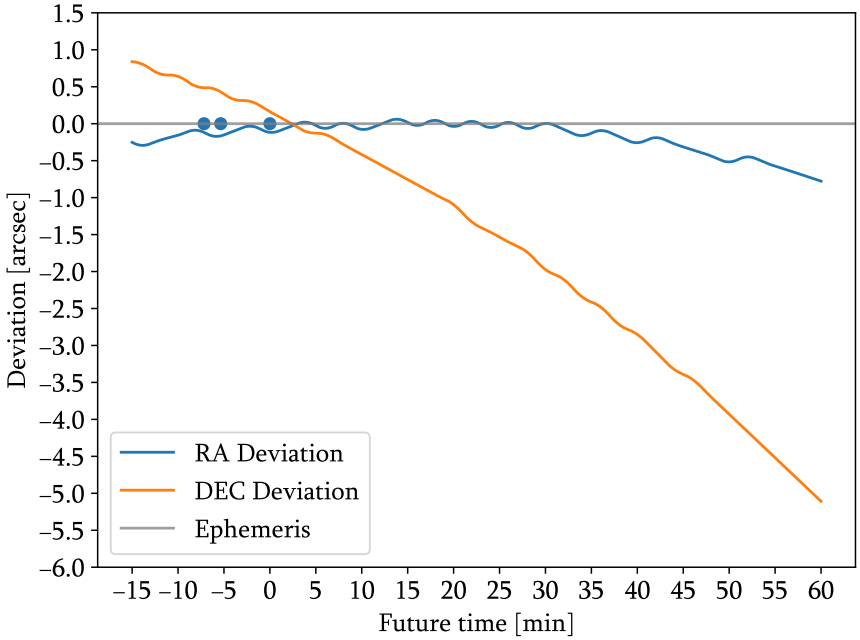

Figure 6: The right ascension and declination deviation between the propagation results and the JPL ephemeris. Using three observations of the asteroid 2022 HB, we computed its on-sky position forward 60 min (and backwards 15 min, for illustrative purposes) by propagating its motion on-sky based on a linear extrapolation of three observations. We compared this result with a computed ephemeris for the same time period from JPL Horizons.[12] The greater deviation in declination over right ascension is specific to this observation of 2022 HB.

(ESA) mission *Gaia*[¶], processed by the *Gaia* Data Processing and Analysis Consortium (DPAC[‖]). Funding for the DPAC has been provided by national institutions, in particular the institutions participating in the *Gaia* Multilateral Agreement. The Pan-STARRS1 Surveys (PS1) have been made possible through contributions of the Institute for Astronomy, the University of Hawaii, the Pan-STARRS Project Office, the Max-Planck Society and its participating institutes, the Max Planck Institute for Astronomy, Heidelberg and the Max Planck Institute for Extraterrestrial Physics, Garching, The Johns Hopkins University, Durham University, the University of Edinburgh, Queen's University Belfast, the Harvard-Smithsonian Center for Astrophysics, the Las Cumbres Observatory Global Telescope Network Incorporated, the National Central University of Taiwan, the Space Telescope Science Institute, the National Aeronautics and Space Administration under Grant No. NNX08AR22G issued through the Planetary Science Division of the NASA Science Mission Directorate, the National Science Foundation under Grant No. AST-1238877, the University of Maryland, and Eotvos Lorand University (ELTE).

REFERENCES

[1] Pieters, C. M. and McFadden, L. A., "Meteorite and asteroid reflectance spectroscopy: Clues to early solar system processes," *Annual Review of Earth and Planetary Sciences* **22**, 457–497 (1994).

[2] DeMeo, F. E., Binzel, R. P., Slivan, S. M., and Bus, S. J., "An extension of the bus asteroid taxonomy into the near-infrared," *Icarus* **202**(1), 160–180 (2009).

[3] Marzari, F., Davis, D., and Vanzani, V., "Collisional evolution of asteroid families," *Icarus* **113**(1), 168–187 (1995).

[4] Cellino, A., Bus, S., Doressoundiram, A., Lazzaro, D., et al., "Spectroscopic properties of asteroid families," *Asteroids III. Univ. of Arizona Press, Tucson* , 633–643 (2002).

[5] Milani, A., Chesley, S. R., and Valsecchi, G. B., "Asteroid close encounters with earth: risk assessment," *Planetary and Space Science* **48**(10), 945–954 (2000).

[¶] https://www.cosmos.esa.int/gaia

[‖] https://www.cosmos.esa.int/web/gaia/dpac/consortium

[6] Rayner, J., Toomey, D., Onaka, P., Denault, A., Stahlberger, W., Vacca, W., Cushing, M., and Wang, S., "Spex: a medium-resolution 0.8–5.5 micron spectrograph and imager for the nasa infrared telescope facility," *Publications of the Astronomical Society of the Pacific* **115**(805), 362 (2003).

[7] Fukugita, M., Shimasaku, K., Ichikawa, T., Gunn, J., et al., "The sloan digital sky survey photometric system," tech. rep., SCAN-9601313 (1996).

[8] Lang, D., Hogg, D. W., Mierle, K., Blanton, M., and Roweis, S., "Astrometry.net: Blind Astrometric Calibration of Arbitrary Astronomical Images," *The Astronomical Journal* **139**, 1782–1800 (May 2010).

[9] Lindegren, L., Hernández, J., Bombrun, A., Klioner, S., Bastian, U., Ramos-Lerate, M., de Torres, A., Steidelmüller, H., Stephenson, C., Hobbs, D., Lammers, U., Biermann, M., Geyer, R., Hilger, T., Michalik, D., Stampa, U., McMillan, P. J., Castañeda, J., Clotet, M., Comoretto, G., Davidson, M., Fabricius, C., Gracia, G., Hambly, N. C., Hutton, A., Mora, A., Portell, J., van Leeuwen, F., Abbas, U., Abreu, A., Altmann, M., Andrei, A., Anglada, E., Balaguer-Núñez, L., Barache, C., Becciani, U., Bertone, S., Bianchi, L., Bouquillon, S., Bourda, G., Brüsemeister, T., Bucciarelli, B., Busonero, D., Buzzi, R., Cancelliere, R., Carlucci, T., Charlot, P., Cheek, N., Crosta, M., Crowley, C., de Bruijne, J., de Felice, F., Drimmel, R., Esquej, P., Fienga, A., Fraile, E., Gai, M., Garralda, N., González-Vidal, J. J., Guerra, R., Hauser, M., Hofmann, W., Holl, B., Jordan, S., Lattanzi, M. G., Lenhardt, H., Liao, S., Licata, E., Lister, T., Löffler, W., Marchant, J., Martin-Fleitas, J. M., Messineo, R., Mignard, F., Morbidelli, R., Poggio, E., Riva, A., Rowell, N., Salguero, E., Sarasso, M., Sciacca, E., Siddiqui, H., Smart, R. L., Spagna, A., Steele, I., Taris, F., Torra, J., van Elteren, A., van Reeven, W., and Vecchiato, A., "Gaia Data Release 2. The astrometric solution," *Astronomy & Astrophysics* **616**, A2 (Aug. 2018).

[10] Chambers, K. C., Magnier, E. A., Metcalfe, N., Flewelling, H. A., Huber, M. E., Waters, C. Z., Denneau, L., Draper, P. W., Farrow, D., Finkbeiner, D. P., Holmberg, C., Koppenhoefer, J., Price, P. A., Rest, A., Saglia, R. P., Schlafly, E. F., Smartt, S. J., Sweeney, W., Wainscoat, R. J., Burgett, W. S., Chastel, S., Grav, T., Heasley, J. N., Hodapp, K. W., Jedicke, R., Kaiser, N., Kudritzki, R. P., Luppino, G. A., Lupton, R. H., Monet, D. G., Morgan, J. S., Onaka, P. M., Shiao, B., Stubbs, C. W., Tonry, J. L., White, R., Bañados, E., Bell, E. F., Bender, R., Bernard, E. J., Boegner, M., Boffi, F., Botticella, M. T., Calamida, A., Casertano, S., Chen, W. P., Chen, X., Cole, S., Deacon, N., Frenk, C., Fitzsimmons, A., Gezari, S., Gibbs, V., Goessl, C., Goggia, T., Gourgue, R., Goldman, B., Grant, P., Grebel, E. K., Hambly, N. C., Hasinger, G., Heavens, A. F., Heckman, T. M., Henderson, R., Henning, T., Holman, M., Hopp, U., Ip, W. H., Isani, S., Jackson, M., Keyes, C. D., Koekemoer, A. M., Kotak, R., Le, D., Liska, D., Long, K. S., Lucey, J. R., Liu, M., Martin, N. F., Masci, G., McLean, B., Mindel, E., Misra, P., Morganson, E., Murphy, D. N. A., Obaika, A., Narayan, G., Nieto-Santisteban, M. A., Norberg, P., Peacock, J. A., Pier, E. A., Postman, M., Primak, N., Rae, C., Rai, A., Riess, A., Riffeser, A., Rix, H. W., Röser, S., Russel, R., Rutz, L., Schilbach, E., Schultz, A. S. B., Scolnic, D., Strolger, L., Szalay, A., Seitz, S., Small, E., Smith, K. W., Soderblom, D. R., Taylor, P., Thomson, R., Taylor, A. N., Thakar, A. R., Thiel, J., Thilker, D., Unger, D., Urata, Y., Valenti, J., Wagner, J., Walder, T., Walter, F., Watters, S. P., Werner, S., Wood-Vasey, W. M., and Wyse, R., "The Pan-STARRS1 Surveys," *arXiv e-prints* , arXiv:1612.05560 (Dec. 2016).

[11] Orbfit Consortium, "OrbFit: Software to Determine Orbits of Asteroids." Astrophysics Source Code Library, record ascl:1106.015 (June 2011).

[12] Giorgini, J. D., Yeomans, D. K., Chamberlin, A. B., Chodas, P. W., Jacobson, R. A., Keesey, M. S., Lieske, J. H., Ostro, S. J., Standish, E. M., and Wimberly, R. N., "JPL's On-Line Solar System Data Service," in [*AAS/Division for Planetary Sciences Meeting Abstracts #28*], *AAS/Division for Planetary Sciences Meeting Abstracts* **28**, 25.04 (Sept. 1996).

[13] Tollestrup, E. V. and Tokunaga, A. T., "New phase compensating secondary mirrors for the nasa infrared telescope facility," in [*Ground-based and Airborne Telescopes III*], **7733**, 559–568, SPIE (2010).

[14] York, D. G., Adelman, J., Anderson Jr, J. E., Anderson, S. F., Annis, J., Bahcall, N. A., Bakken, J., Barkhouser, R., Bastian, S., Berman, E., et al., "The sloan digital sky survey: Technical summary," *The Astronomical Journal* **120**(3), 1579 (2000).

[15] Kaiser, N., Aussel, H., Burke, B. E., Boesgaard, H., Chambers, K., Chun, M. R., Heasley, J. N., Hodapp, K.-W., Hunt, B., Jedicke, R., et al., "Pan-starrs: a large synoptic survey telescope array," in [*Survey and Other Telescope Technologies and Discoveries*], **4836**, 154–164, International Society for Optics and Photonics (2002).

[16] Spoto, F., Payne, M., Holman, M., and Vereš, P., "The new MPC NEO Confirmation Page: improvements and results," in [*7th IAA Planetary Defense Conference*], 31 (Apr. 2021).

[17] Cuillandre, J.-C., Magnier, E. A., Isani, S., Sabin, D., Knight, W., Kras, S., and Lai, K., "Cfht's skyprobe: a real-time sky-transparency monitor," in [*Observatory Operations to Optimize Scientific Return III*], **4844**, 501–507, International Society for Optics and Photonics (2002).